A Novel Analysis, Design, and Optimal Methodology of High-Frequency Oscillation for Dual Active Bridge Converters With WBG Switching Devices and Nanocrystalline Transformer Cores

Bin Cui, *Member, IEEE*, Hongliang Shi, *Student Member, IEEE*, Qianhao Sun, *Student Member, IEEE*, Xueteng Tang, Lucheng Hong, *Member, IEEE*, and Biao Zhao, *Senior Member, IEEE*

***Abstract*—With the fast development of advanced switches and magnetic cores, high-frequency oscillation (HFO) caused by high *dv/dt* of fast switching devices and stray capacitances of transformer in dual active bridge (DAB) presents a significantly challenge. In this article, a comprehensive analysis, design, and optimal methodology of HFO for DAB with wideband gap (WBG) switching devices and nanocrystalline transformer cores is proposed. The stray parameters equivalent circuit of DAB is built and the key influencing factors to mitigated the HFO are identified by establishing a time-domain analytical model. Based on the theoretical analysis, this article points out for the first time that the traditional method of decreasing the stray capacitance of the transformer to eliminate HFO is not suitable for high *dv/dt* occasions when using WBG switching devices. Correspondingly, a novel elimination method of HFO by equating the voltage changing time of *dv/dt* to the oscillation cycle is proposed, through which the minimum voltage spike amplitude (VSA) of HFO can be achieved mathematically. A 6.6-kW DAB prototype with three different transformers is developed and an approximately 95% reduction of the VSA can be achieved when the proposed HFO elimination method is adopted, which verifies the effectiveness of the proposed method.**

***Index Terms*—Dual active bridge (DAB), elimination method, high-frequency oscillation (HFO), stray capacitance.**

I. Introduction

THE dual active bridge (DAB) based dc–dc converter with intermediate high-frequency isolation transformer is the key equipment in dc–dc applications as it can achieve a large scale of power transmission with flexible control features, while guaranteeing the bilateral galvanic isolation at the same time [1], [2]. With the increased switching frequency, the volume and weight of the transformer will be significantly reduced [3], [4], shedding a shrewder insight into traction, aircraft, and electric vehicle areas [5]. The growing trend of high switching frequency development in DAB converter benefits a lot from the new materials of Fe-based nanocrystalline alloys and Silicon Carbide (SiC) power devices [3]. Fe-based nanocrystalline alloy is considered as the most promising material of high-frequency transformer cores for its higher saturation, lower losses, and higher curie temperature characteristics, while unlike the ferrite cores, the nanocrystalline cores with high electrical conductivity characteristics can considerably increase the transformer's stray capacitances [4], [6], [7]. As for the SiC power devices, when being used in DAB to achieve a lower switching losses or higher switching frequency, a higher *dv/dt* (usually around 50–100 kV/μs [8]) on the H-bridge output voltage would be produced, which stimulates the high-frequency oscillation (HFO) between the stray capacitances of the transformer and the inductive components on the ac side of the DAB converters [9]–[11].

The unexpected voltage and current ringing, i.e., HFO phenomenon, post severe threats to the converter's performance. On the one hand, the frustrating voltage spikes on the transformer ports pump up the isolation demand, more insulation materials are therefore needed to cope with the high-voltage stresses [12]. The additional insulation materials then further thwart the heat dissipation and decrease the power density of the transformer. On the other hand, the undesired HFO phenomenon could distort the voltage and current waveforms, contributes to electromagnetic interference (EMI) and common mode noise problems, increase high-frequency losses[13], and reduces the overall efficiency and reliability of the converters [9], [10], [12], [14]. The background and threats of HFO are explicitly illustrated in Fig. 1. It is of great necessity to eliminate the HFO and improve the aforementioned operating performance of the DAB converters.

Since the parasitic capacitances of the transformer is regarded as the major factor causing the HFO phenomenon, many efforts have been made to evaluate the capacitive effects of the transformer [6], [7], [15]. As the electric potentials between turns,

Manuscript received June 17, 2020; revised August 30, 2020 and October 31, 2020; accepted December 19, 2020. Date of publication January 5, 2021; date of current version March 5, 2021. This work was supported by the National Natural Science Foundation of China under Grant 52007097. Recommended for publication by Associate Editor X. Wu. *(Corresponding authors: Lucheng Hong and Biao Zhao.)*

Bin Cui, Qianhao Sun, Xueteng Tang, and Biao Zhao are with the Department of Electrical Engineering, Tsinghua University, Beijing 100084, China (e-mail: cuibin@tsinghua.edu.cn; sxsunqianhao@163.com; tangxueteng@126.com; zhaobiao@tsinghua.edu.cn).

Hongliang Shi is with the CRRC ZHUZHOU ELECTRIC CO., LTD., Zhuzhou 412001, China (e-mail: shihl1@csrzic.com).

Lucheng Hong is with the Department of Electrical Engineering, Southeast University, Nanjing 210096, China (e-mail: hlc3061@seu.edu.cn).

Color versions of one or more of the figures in this article are available online at https://doi.org/10.1109/TPEL.2021.3049140.

Digital Object Identifier 10.1109/TPEL.2021.3049140

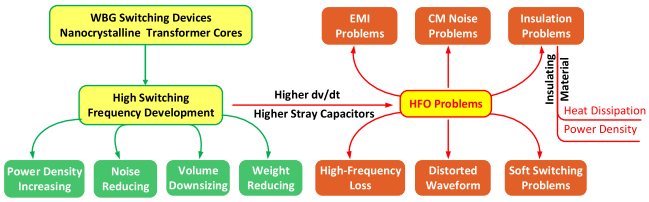

Fig. 1. Background and threats of HFO in DAB converters.

winding layers, cores, and shielding layers of the transformer create these stray capacitances [6], a capacitance matrix can be used to build the refined model of the transformer to characterize the electric field coupling effects between different parts of the transformer [16], [17]. However, the capacitance matrix model contains hundreds of circuit parameters, which brings great complexity for further theoretical analysis [18], [19]. On the contrary, the lumped parameter model with a limited number of equivalent stray capacitances of the transformer can be established from the perspective of the external characteristics of the transformer. For a two windings transformer, one-capacitance [20], three-capacitance [21]–[23], six-capacitance [12], and ten-capacitance [7] stray capacitances equivalent circuit are proposed with different degrees of independent voltage freedom [24], among which, the π-shaped three stray capacitance equivalent circuit is widely used for the purpose of dynamic circuit modeling when taking the transformer as a two-port system from the magneto static perspective. Various methods have been proposed to extract the stray capacitances of the transformer, such as analytical formula [6], [15], numerical methods [7], [8], [12], or experimental measurements [20], [25], among which, the experimental extraction method based on the self-resonant frequencies of the transformer is widely accepted for its practicality and accuracy [21], [25].

To mitigate the HFO in the dc–dc converter, different winding arrangements and constructions of the transformer have been proposed by reducing the stray capacitances with the aid of analytical formula or finite-element analysis [10], [12], [14], claiming that the HFO problem could be significantly alleviated with lower stray capacitances. However, the stray capacitance of the transformer could not be radically eradicated, because electric field energy in the transformer cannot be completely removed. Some scholars have pointed out that the current ringing in DAB converter can be mitigated when the phase-shifting inductors of DAB converter are placed on both sides of the transformer [26], or putting the phase-shifting inductor on the low-voltage side of the DAB converter especially when the transformer has a large transformation ratio [27]. However, these methods have no effect on voltage ringing of the transformer. On the other hand, the stray capacitance of the transformer can be gainfully utilized as a part of a resonant network [28], resulting in improved power density of the converter. But, the accuracy of stray capacitance is very difficult to be precisely controlled.

From above, minimizing the stray capacitances of the transformer is a key method to eliminate the HFO in dc–dc converters. However, there is a contradiction between the stray capacitance and the leakage inductance of the transformer [29]. The smaller the stray capacitance is, the larger the leakage inductance is, which means it is impossible to achieve the minimum stray capacitance and minimum leakage inductance at the same time by optimizing the physical parameters of the transformer. It is well recognized that three factors mainly determine the self-capacitance of the transformer [6]: 1) the dielectric constant of the insulating materials; 2) the geometry of windings and cores; and 3) the arrangement and connecting strategy of windings. Generally, the multisection winding arrangement technique has been widely employed in order to reduce the stray capacitances by improving the voltage distribution of the transformer windings [15], [30] and a minimum self-capacitance layout design can be achieved with single winding layer of the transformer, as the most critical electric field energy between layers of the transformer is eliminated.

Although several mitigation strategies to mitigate the HFO are proposed to improve the converter performance, the existing research still fails to: 1) identify all the key influencing factors of the HFO mathematically by establishing a time-domain model of HFO; 2) deriving the functional relationship between the stray capacitances of the transformer and the voltage spike amplitude (VSA) of the HFO; and 3) propose a fundamental HFO elimination method theoretically.

In this article, a time-domain analytical model of HFO is first established based on the stray parameters equivalent circuit of DAB, by which the key influencing factors to mitigate the HFO are identified. Mathematical derivation is deduced with the conclusion that HFO can be mitigated by reducing the capacitance of the transformer, however, it will lose effect in the case of fast switching devices are adopted or high *dv*/*dt* are produced in the DAB converters. A novel elimination method of HFO is proposed by equating the voltage changing time of *dv*/*dt* and the oscillation cycle theoretically. The corresponding experimental verifications are conducted on a 6.6-kW DAB prototype, showing an approximately 95% reduction of the VSA can be achieved with the proposed HFO elimination method adopted in this article.

II. Proposed Equivalent Circuit and Time-Domain Analytical Modeling of HFO in DAB

A. HFO Mechanism Analysis in DAB With WBG Switch and Nanocrystalline Transformer

An ideal circuit schematic of DAB converter is shown in Fig. 2(a), which comprises a primary H-Bridge (H_1), a secondary H-Bridge (H_2), a high-frequency transformer (T_1), and two phase-shift inductors ($L_{\rm ph1}$ and $L_{\rm ph2}$), which are symmetrically placed on the primary and secondary sides of the transformer. The transmitted power of the DAB converter can be controlled by adjusting the phase-shifting angle of D between the ac voltage of the primary H-bridge (U_{H1}) and secondary H-bridge (U_{H2}).

However, in an actual circuit, the fast changing of U_{H1} during the transient switching states of DAB convertors, referred as *dv*/*dt*, has plentiful harmonic components even up to several megahertz (MHz), making the electric coupling effect of the transformer becomes as important as the magnetic coupling effect. Therefore, the stray capacitance of the transformer cannot be ignored, and a complicated high-order stray parameters network at the ac side of the DAB converter can be generated. When investigating the harmonic analysis characteristics of

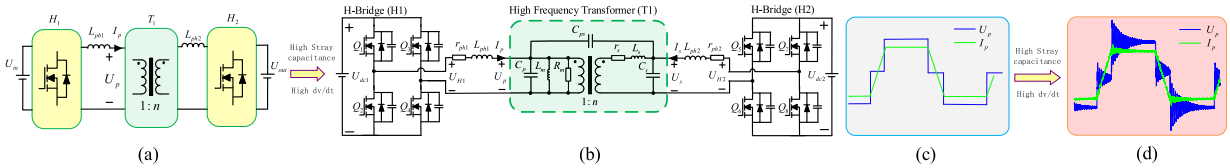

Fig. 2. Circuit schematic and waveforms of the transformer in DAB converters. (a) Ideal circuit schematic of a DAB converter. (b) Actual circuit diagram of a DAB converter with stray parameters. (c) Ideal voltage and current waveforms of the transformer. (d) Experimental voltage and current waveforms of the transformer.

a high-frequency transformer where the concerned frequency is not very high, that is, the propagation delay effect can be reasonable ignored (usually below several MHz which are concerned in this article), the magnetic and capacitive effects of the transformer can be equivalent to lumped parameters models which focused on winding level. Among these lumped parameters models, the π-shaped three stray capacitance equivalent circuit is widely used for dynamic circuit modeling, which is also employed in this article to characterize the electrical coupling effect of the transformer in the DAB converter as shown in Fig. 2(b), where C_p is the self-capacitances of the primary windings, C_s is the self-capacitances of the secondary windings, $C_{\rm ps}$ is the mutual capacitance between the primary and the secondary windings, L_m is the magnetizing inductance, R_m is the magnetizing resistance referred to the primary side, L_s is the leakage inductance referred to the secondary side, r_s is the ac resistance of the transformer winding referred to the secondary side, and n is the turn ratio of the transformer.

The ideal voltage and current waveforms of the transformer (i.e., U_p and I_p) when ignoring the stray capacitances of the transformer are shown in Fig. 2(c). Correspondingly, the experimental voltage and current waveforms in an actual DAB converter are shown in Fig. 2(d). It can be seen that the voltage and current waveforms of the transformer is seriously distorted in an actual DAB converter when taking the stray capacitance of the transformer into consideration. A severe HFO problem in the stray parameters network of DAB converter is generated. The oscillation frequency of the HFO is up to several MHz, causing EMI, high-frequency loss, and isolation failure problems, which seriously threatens the safety and reliability of the DAB converter. In recent years, with the wideband gap (WBG) switching devices and Fe-based nanocrystalline alloys utilized in DAB converters, the HFO at the ac side of the DAB converter becomes to be an inevitable and urgent problem to be solved.

B. Equivalent Circuit of Stray Parameters Network

As the transient response of a high-order stray parameters network cannot be solved mathematically, the order of that needs to be reasonably reduced. First, considering that the leakage inductance L_s is much smaller than the magnetizing inductance L_m, the stray capacitances of the transformer can be referred to the primary side as shown in Fig. 3. Therefore, the primary referred stray capacitances of C_1, C_2, and C_3 can be expressed as follows [20]:

$$\begin{cases} C_1 = C_p - (n-1)C_{\rm ps} \\ C_2 = n^2 C_s + n(n-1)C_{\rm ps} \\ C_3 = nC_{\rm ps}. \end{cases} \tag{1}$$

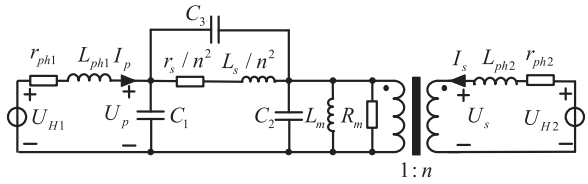

Fig. 3. Stray parameters network at the ac side of the DAB converter with the stray capacitance of the transformer referred to the primary side.

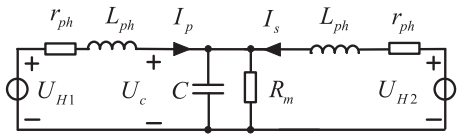

Fig. 4. Simplified circuit of the stray parameters network at the ac side of the DAB converter.

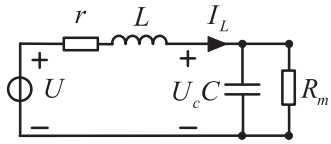

Fig. 5. Thevenin equivalent circuit of the stray parameters network at the ac side of the DAB converter.

Generally, as the magnetizing inductance is much larger than the phase-shift inductance, and the leakage inductance is always designed to be very small to increase the maximum transmission power of a DAB converter, the stray parameters network shown in Fig. 3 can be simplified as shown in Fig. 4 [20]. The simplified stray capacitance of C can be expressed as

$$C = C_1 + C_2. \tag{2}$$

As the phase-shift inductors are symmetrically placed on both sides of the transformer, the following equations should be met to realize a symmetrical structure:

$$\begin{cases} L_{\rm ph} = L_{\rm ph1} = \frac{L_{\rm ph2}}{n^2} \\ r_{\rm ph} = r_{\rm ph1} = \frac{r_{\rm ph2}}{n^2} \end{cases} \tag{3}$$

where $L_{\rm ph}$ is the phase-shift inductance and $r_{\rm ph}$ is the resistance of the phase-shift inductor in the simplified circuit of Fig. 4.

From Fig. 4, a Thevenin equivalent circuit can be obtained as shown in Fig. 5 according to Thevenin's theorem. The

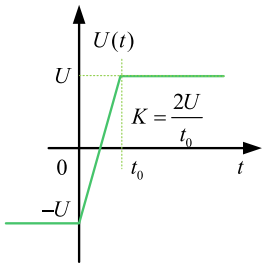

Fig. 6. Mathematical model of *dv*/*dt* in time domain.

corresponding circuit parameters are shown as (4)

$$\begin{cases} L = \frac{L_{\rm ph}}{2} \\ r = \frac{r_{\rm ph}}{2} \\ I_L = I_p + I_s \\ U = \frac{U_{H1}+U_{H2}}{2} \end{cases} \tag{4}$$

where L is the phase-shift inductance, r is the resistance of the phase-shift inductor, I_L is the current of the phase-shift inductor, and U is the voltage source in the Thevenin equivalent circuit of Fig. 5.

It can be seen that the high-order stray parameters network at the ac side of the DAB converter can be simplified to a second-order equivalent circuit as shown in Fig. 5, from which, the circuit responses during the transient switching states of DAB convertors can be solved mathematically.

C. Time-Domain Analytical Model of HFO

The *dv*/*dt* of the converter can be modeled by a segmental linear function as shown in Fig. 6, which can be expressed mathematically by

$$U(t) = K[t\varepsilon(t) - (t-t_0)\varepsilon(t-t_0)] - U \tag{5}$$

where $\varepsilon(t)$ is a unit step function, t_0 is the voltage changing time of *dv*/*dt*, and K is the voltage changing rate of *dv*/*dt*.

When taking the voltage changing time of U_{H2} (from negative to positive) as the initial time, the ac voltage of H-bridge (i.e., U_{H1} and U_{H2}) can be expressed as follows:

$$\begin{cases} U_{H1}(t) = U_{\rm dc1} \\ U_{H2}(t) = Kt\varepsilon(t) - K(t-t_0)\varepsilon(t-t_0) - U_{dc2} \end{cases} \tag{6}$$

where the voltage changing rate of *dv*/*dt* can be expressed as

$$K = \frac{dv}{dt} = \frac{2U_{\rm dc2}}{t_0}. \tag{7}$$

The voltage source in the Thevenin equivalent circuit of Fig. 5 can be expressed as

$$U(t) = \frac{U_{H1}(t) + U_{H2}(t)}{2} = kt\varepsilon(t) - k(t-t_0)\varepsilon(t-t_0) \tag{8}$$

where $k = \frac{K}{2}$ is the *dv*/*dt* of Thevenin equivalent circuit in Fig. 5.

Solving the zero-input and zero-state response separately and add them together to obtain the complete circuit response is a simple method for transient circuits solution. In the first place, zero-state response is a circuit response due to the input system excitation source (with initial conditions of the circuit set to zero). The voltage source of $U(t)$ in (8) can be departed into two ramp functions shown as follows based on the superposition theorem:

$$\begin{cases} U(t) = U\_1(t) - U\_2(t) \\ U\_1(t) = kt\varepsilon(t) \\ U\_2(t) = kt\varepsilon(t-t_0). \end{cases} \tag{9}$$

Taking the excitation source of $U\_1(t)$ as an example, the zero-state voltage equation in complex frequency domain can be derived as follows:

$$\begin{cases} (\frac{1}{sL+r} + sC + \frac{1}{R_m})U_{c1\_1}(s) = \frac{U\_1(s)}{sL+r} \\ U\_1(s) = \frac{k}{s^2} \end{cases} \tag{10}$$

from which, the network function of $H(s)$ can be derived as

$$\begin{aligned} H(s) &= \frac{U_{C1\_1}(s)}{U\_1(s)} \\ &= \frac{1}{LC[s^2 + (\frac{r}{L} + \frac{1}{CR_m})s + \frac{r+R_m}{LCR_m}]}. \end{aligned} \tag{11}$$

There are two poles in $H(s)$, which can be deduced as

$$\begin{cases} P_1 = -\frac{rCR_m+L}{2LCR_m} + \sqrt{(\frac{rCR_m+L}{2LCR_m})^2 - \frac{r+R_m}{LCR_m}} \\ P_2 = -\frac{rCR_m+L}{2LCR_m} - \sqrt{(\frac{rCR_m+L}{2LCR_m})^2 - \frac{r+R_m}{LCR_m}}. \end{cases} \tag{12}$$

The oscillation in the circuit will be definitely generated when these two poles is formed into a pair of conjugate complex root, which means the following inequality could be established:

$$\left(\frac{rCR_m+L}{2LCR_m}\right)^2 - \frac{r+R_m}{LCR_m} < 0. \tag{13}$$

When using α and β represent the real and imaginary parts of the poles as shown in the following:

$$\begin{cases} \alpha = -\frac{rCR_m+L}{2LCR_m} \\ \beta = \sqrt{\frac{r+R_m}{LCR_m} - (\frac{rCR_m+L}{2LCR_m})^2} \end{cases} \tag{14}$$

the poles of $H(s)$ can be simply expressed as

$$\begin{cases} P_1 = -\alpha + i\beta \\ P_2 = -\alpha - i\beta. \end{cases} \tag{15}$$

From (10), the zero-state response in complex frequency domain can be solved as follows:

$$U_{C1\_1}(s) = \frac{\frac{k}{s^2}}{LC[s^2 + (\frac{r}{L} + \frac{1}{CR_m})s + \frac{r+R_m}{LCR_m}]}. \tag{16}$$

The corresponding zero-state response in time domain can be solved by Laplace inverse transformation as follows:

$$\begin{aligned} U_{C1\_1}(t) = \frac{k}{LC}\Bigg[&\frac{1}{\beta(\alpha^2+\beta^2)}e^{\alpha t}\cos(\beta t + \theta_{1\_1}) \\ &+ \frac{t}{\alpha^2+\beta^2} + \frac{2\alpha}{(\alpha^2+\beta^2)^2}\Bigg] \end{aligned} \tag{17}$$

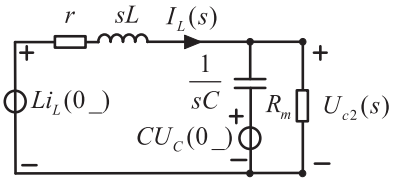

Fig. 7. Circuit diagram for solving the zero-input state of the circuit in complex frequency domain.

where

$$\theta_{1\_1} = \operatorname{arctg}\left(\frac{\alpha^2-\beta^2}{2\alpha\beta}\right). \tag{18}$$

The zero-state response excited by the second part of the voltage source $U_{\_2}(t)$ can be drawn directly based on delay theorem shown as follows for $U_{\_2}(t)$ is a function delayed by the first part of excitation source $U_{\_1}(t)$ for a time interval of t_0:

$$\begin{aligned} U_{C1\_2}(t) &= U_{C1\_1}(t-t_0) \\ &= \frac{k}{LC}\left[\frac{1}{\beta(\alpha^2+\beta^2)}e^{\alpha t}e^{-\alpha t_0}\cos(\beta(t-t_0)+\theta_{1\_1})\right. \\ &\quad \left. + \frac{(t-t_0)}{\alpha^2+\beta^2} + \frac{2\alpha}{(\alpha^2+\beta^2)^2}\right]. \end{aligned} \tag{19}$$

Therefore, the complete zero-state response of $U_{c1}(t)$ can be derived by adding (17) and (19) based on superposition theorem as

$$\begin{aligned} U_{C1}(t) &= U_{C1\_1}(t) - U_{C1\_2}(t) \\ &= A_1 e^{\alpha t}\cos(\beta t+\theta_1) + \frac{k}{LC}\frac{t_0}{\alpha^2+\beta^2}. \end{aligned} \tag{20}$$

During which

$$\begin{cases} A_1 = \frac{k}{LC}\frac{1}{\beta(\alpha^2+\beta^2)}\sqrt{1+e^{-2\alpha t_0}-2e^{-\alpha t_0}\cos\beta t_0} \\ \theta_1 = \arctan\left(\frac{\sin\theta_{1\_1}-e^{-\alpha t_0}\sin(\theta_{1\_1}-\beta t_0)}{\cos\theta_{1\_1}-e^{-\alpha t_0}\cos(\theta_{1\_1}-\beta t_0)}\right). \end{cases} \tag{21}$$

It can be seen from (20) that the zero-state response $U_{c1}(t)$ is formed by two parts: the first part is an exponentially attenuating oscillation function with A_1 as the oscillation amplitude, α as the attenuation coefficient, and β as the oscillation angular frequency; the second part is a time-independent constant value, determined by the *dv*/*dt* and parameters of the circuit network. Meanwhile, it can be seen from (21) that the oscillation amplitude of A_1 is determined by *dv*/*dt* and the circuit network parameters of DAB; while α and β are solely determined by the circuit network parameters, reflecting the inherent oscillation properties of the resonant network, regardless of the forms of the excitation source.

Different from zero-state response, the zero-input response of the circuit is due to the circuit initial conditions alone (with the input excitation source being set to zero). In order to evaluate the influence of initial circuit conditions (that is, the initial current of the inductor and the initial voltage of the capacitor), the zero-input response of U_{c2} (t) is solved as follows.

A circuit diagram for solving zero-input state response can be drawn as shown in Fig. 7.

The circuit voltage equation in Fig. 7 can be derived as

$$\left(\frac{1}{sL+r}+sC+\frac{1}{R_m}\right)U_{C2}(s) = \frac{Li_L(0\_)}{sL+r} + CU_C(0\_) \tag{22}$$

from which, the zero-input response of the circuit $U_{c2}(s)$ in complex frequency domain can be solved as follows:

$$U_{C2}(s) = \frac{sU_C(0\_)+\frac{r}{L}U_C(0\_)+\frac{1}{C}i_L(0\_)}{s^2+(\frac{r}{L}+\frac{1}{CR_m})s+\frac{r+R_m}{LCR_m}}. \tag{23}$$

The corresponding zero-input response in time domain can be solved by Laplace inverse transforming as follows:

$$U_{C2}(t) = A_2 e^{\alpha t}\cos(\beta t+\theta_2) \tag{24}$$

during which

$$\begin{cases} A_2 = \sqrt{{U_C}^2(0\_)+\frac{1}{\beta^2}[(\alpha+\frac{r}{L})U_C(0\_)+\frac{1}{C}i_L(0\_)]^2} \\ \theta_2 = \arctan\left[\frac{-1}{\beta}\left(\alpha+\frac{r}{L}+\frac{1}{C}\frac{i_L(0\_)}{U_C(0\_)}\right)\right]. \end{cases} \tag{25}$$

It can be seen from (24) that, different from $U_{c1}(t)$, the zero-input response of $U_{c2}(t)$ is only formed by one part: an exponentially attenuating oscillation function with A_2 as the oscillation amplitude, α as the attenuation coefficient, and β as the oscillation angular frequency. Meanwhile, it can be seen from (25) that A_2 is determined by the initial current of the inductor $i_L(0\_)$, the initial voltage of the capacitor $U_C(0\_)$, and the circuit network parameters at the same time.

Finally, the complete response $U_c(t)$ can be simply drawn by adding the zero-state response of $U_{c1}(t)$ and zero-input response of $U_{c2}(t)$ as follows:

$$\begin{aligned} U_C(t) &= U_{C1}(t) + U_{C2}(t) \\ &= Ae^{\alpha t}\cos(\beta t+\theta) + \frac{k}{LC}\frac{t_0}{\alpha^2+\beta^2} \end{aligned} \tag{27}$$

during which

$$\begin{cases} A = \sqrt{A_1^2+A_2^2+2A_1A_2\cos(\theta_1+\theta_2)} \\ \theta = \arctan\left(\frac{A_1\sin(\theta_1)+A_2\sin(\theta_2)}{A_1\cos(\theta_1)+A_2\cos(\theta_2)}\right). \end{cases} \tag{28}$$

It can be seen from (27) that the complete circuit response of $U_c(t)$ is formed by two parts. The first one is an exponentially attenuating oscillation function with *A* as the oscillation amplitude (i.e., the VSA of the HFO), α as the attenuation coefficient, and β as the oscillation angular frequency. The second one is a time-independent constant value, determined by the *dv*/*dt* and parameters of the circuit network. Meanwhile, it can be seen from (28) that the oscillation amplitude of *A* is determined by the zero-input and zero-state response of the circuit simultaneous.

D. Verification of the Circuit Responses

In order to verify the correctness of the complete circuit response of $U_c(t)$ derived above, a simulation model of DAB converter based on LTspice is built with the circuit diagram shown in Fig. 2(b) and the circuit parameters listed in Tables I and II in Section V.

The simulation voltage waveforms and the theoretical waveforms of the circuit responses at the transient switching states

TABLE I
SPECIFICATIONS AND PARAMETERS OF DAB PROTOTYPE

Symbol	Parameters	Value
U_{dc1}	Rated input voltage	600 VDC
U_{dc2}	Rated output voltage	600 VDC
P	Rated power	6.6 kW
f_s	Switching frequency	40 kHz
L_{ph1} ,L_{ph2}	Phase-shift inductor	60.51 μH
r_{ph1} ,r_{ph2}	Resistance of Phase-shift inductor	0.016 Ω
D	Phase-shift angle at rated power	0.25

TABLE II
STRAY PARAMETERS OF TRANSFORMER

Symbol	Parameters	# 1	# 2	# 3
C_p	Primary capacitance	99.7 pF	51.2 pF	39.1 pF
C_s	Secondary capacitance	99.7 pF	51.2 pF	39.1 pF
C_{ps}	Mutual capacitance	381 pF	166 pF	129 pF
L_m	Magnetizing inductance	251 mH	63 mH	63 mH
r_s	Winding resistance	0.07 Ω	0.04Ω	0.04 Ω
L_s	Leakage inductance	14.2 μH	5.1 μH	5.1 μH
R_m	Magnetizing resistance	43 kΩ	12 kΩ	12 kΩ
n	Transformer ratio	1:1	1:1	1:1

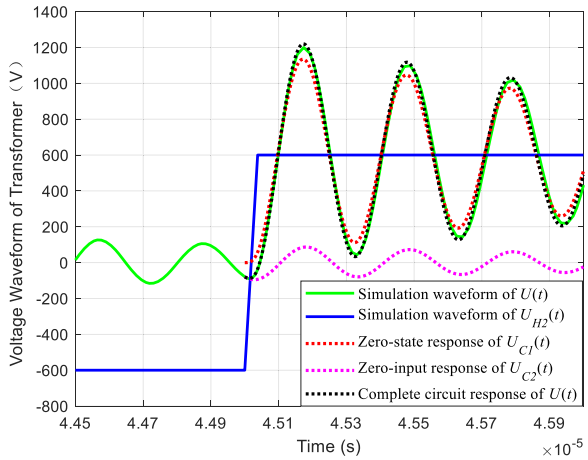

Fig. 8. Comparison between the simulation and theoretical voltage oscillation waveforms of the DAB converter.

of DAB convertors are drawn in Fig. 8 simultaneously. It can be seen that the zero-input response of $U_{c2}(t)$ (pink dotted line shown in Fig. 8) can be regarded as a continuation of the initial oscillation voltage waveform of the transformer (green solid line before switching transient time), which is mainly determined by the initial circuit conditions. The zero-state response of $U_{c1}(t)$, (red dotted line shown in Fig. 8) is stimulated by the *dv/dt* of the DAB converter at the switching transient time of DAB convertor, regardless of the initial circuit conditions. The complete response of $U_c(t)$ (black dotted line shown in Fig. 8) is determined by the zero-input and zero-state response of the circuit together. The peak voltage of the simulation voltage waveform is up to 1200 V where the peak voltage of the theoretical voltage waveform is 1210 V with a relative error of 0.8%. This error may be caused by the order reduction process of the stray parameter circuit analyzed shown above. The consistency between the simulated waveform and the theoretical waveform verifies the correctness of the complete response of $U_c(t)$ described by (27) and (28).

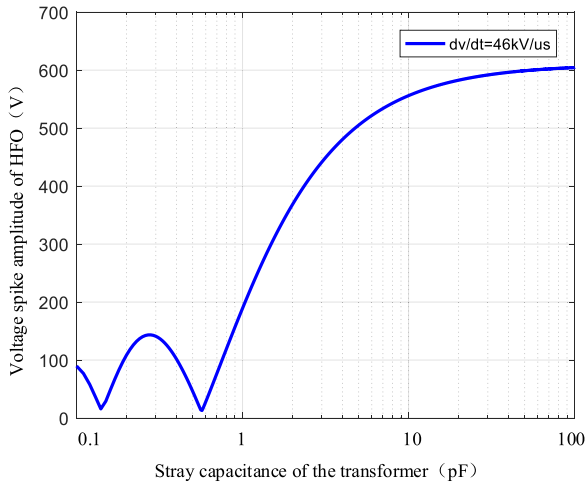

Fig. 9. Mathematical functional relationship between the VSA of HFO (A) and the stray capacitance of the transformer (C) in the DAB prototype.

III. COMPREHENSIVE ANALYSIS WITH UNIVERSAL INFLUENCING FACTORS OF HFO

As is established in (28),the VSA of the HFO (A) is determined by many influencing factors, including the stray capacitance of the transformer (C), the *dv/dt* of the converter (k), the excitation resistance of the transformer (R_m), the ac resistance of the transformer (r), the phase-shift inductance (L), the initial current of the phase-shifting inductor $i_L(0\_)$, and the initial voltage of the transformer's stray capacitance $U_C(0\_)$. The key influencing factors of the HFO can be identified mathematically based on the time-domain analytical model of HFO shown in Section II as follows.

A. Stray Capacitance of the Transformer

The mathematical functional relationship between the VSA of HFO (A) and the stray capacitance of the transformer (C) can be shown in Fig. 9, which is drawn based on (28) and the circuit parameters of a DAB prototype in Section V. Particularly, the *dv/dt* of the DAB prototype is 46 kV/μs, which is measured from the experiment.

It can be seen from Fig. 9 that there is a nonlinear relationship between the VSA of HFO and the stray capacitance of the transformer. The VSA of the HFO is up to 600 V when the stray capacitance of the transformer is 100 pF, and decreased to nearly 0 V when the stray capacitance is reduced to 0.56 pF, while inversely goes up to about 143 V when the stray capacitance is further reduced to 0.27 pF. The stray capacitance of the transformer is not the smaller the better to mitigate the HFO, which is different from the traditional ideas in the existing literatures.

In practice, the stray capacitance of the transformer is very difficult to be controlled, and the minimum stray capacitance of the transformer could merely be reduced to dozens of pF with the optimized transformer constructions and winding arrangements.

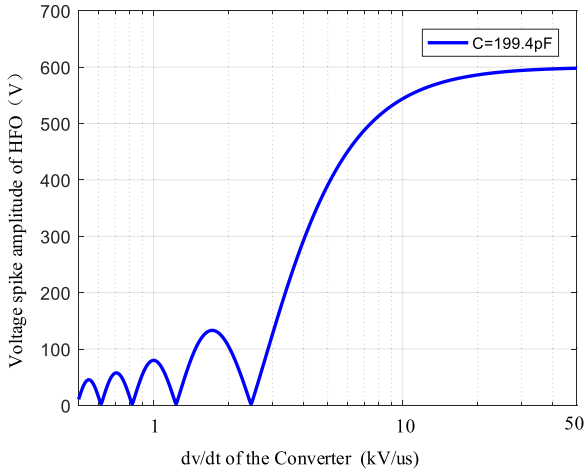

Fig. 10. Mathematical functional relationship between the VSA of HFO (A) and the dv/dt of the converter (k) in the DAB prototype.

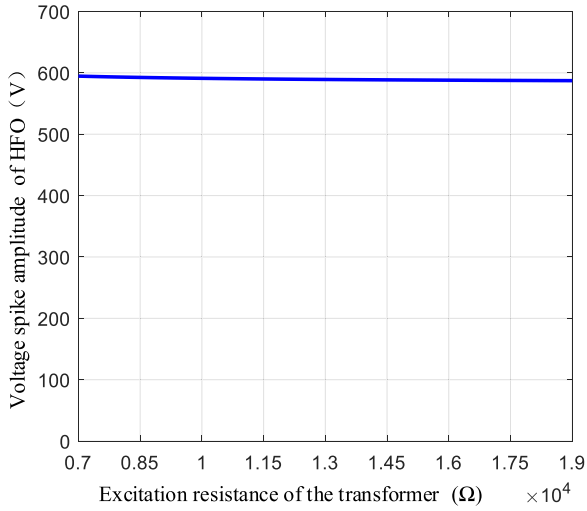

Fig. 11. Mathematical functional relationship between the VSA of HFO (A) and the excitation resistance of the transformer (R_m) in the DAB prototype.

However, taking the DAB prototype in this article as an example, only when the stray capacitance of the transformer is less than 10 pF, the VSA of HFO could be significantly suppressed. It is almost impossible to get such a small stray capacitance for an actual transformer, which means that the traditional elimination method of HFO by decreasing the stray capacitance of the transformer is not suitable to the DAB prototype built in this article, for the WBG devices of SiC-MOSFETs are utilized and an extremely high dv/dt is generated.

B. dv/dt *of the Converter*

The mathematical functional relationship between the VSA of HFO (A) and the dv/dt of the converter (k) can be drawn as shown in Fig. 10 based on (28) and the circuit parameters in Section V as listed in Tables I and II.

It can be seen from Fig. 10 that there is also a nonlinear relationship between the VSA of HFO and the dv/dt of the converter. The VSA of the HFO is up to 600 V when the dv/dt of the converter is 10 kV/μs, and will decrease to nearly 0 V when the dv/dt is reduced to 2.46 kV/μs, while inversely goes up to about 133 V when the dv/dt is further reduced to 1.73 kV/μs. The dv/dt of the converter is not the smaller the better to mitigate the HFO, which is also different from the traditional ideas.

In practice, when WBG switching devices such as SiC-MOSFETs are used, HFO in the DAB converters is an inevitable and urgent problem to be solved, because the dv/dt of the converter can be almost reached up to 30–50 kV/μs [10] due to the fast voltage changing characteristics of the H-bridge. However, the nonlinear relationship between the VSA and dv/dt together with the nonlinear relationship between VSA and C makes it extremely difficult and complicated to seek effective elimination method of HFO in a specific DAB prototype.

C. Excitation Resistance of the Transformer

As the excitation resistance of the transformer (R_m) is determined by the core loss characteristics and the maximum magnetic field amplitude of the transformer cores, different transformers will have different excitation resistances. In order to evaluate whether R_m is a key influencing factor of the HFO, the mathematical functional relationship between the VSA of HFO (A) and the excitation resistance of the transformer (R_m) can be drawn in Fig. 11 based on (28) and the circuit parameters in Section V.

It can be seen from Fig. 11 that the VSA of HFO almost does not change with R_m, that is to say, R_m is not a key influencing factor of HFO for the DAB prototype in this article.

D. AC Resistance of the Transformer

As to the ac resistance of the transformer (r), which is mainly determined by the winding wire gauges and the skin effect of the transformer windings under the oscillation frequency of several MHz, different transformers will have different ac resistances under the oscillation frequency. In order to evaluate whether r is a key influencing factor of the HFO, the mathematical functional relationship between the VSA of HFO (A) and the ac resistance of the transformer (r) can also be drawn in Fig. 12 based on (28) and the circuit parameters in Section V.

It can be seen from Fig. 12 that the VSA of HFO almost does not change with r, and r is also not a key influencing factor of HFO for the DAB prototype.

E. Other Possible Influencing Factors of HFO

It is well recognized that the circuit parameter of phase-shift inductance (L) is determined by the rated transmission power of the DAB converters, and cannot be a variable value once the circuit parameters of DAB converter are confirmed. Therefore, the phase-shift inductance (L) cannot be an adjustable parameter to solve the HFO problems. As to the initial current of the phase-shifting inductor $i_L(0\_)$ and the initial voltage of the transformer's stray capacitance $U_C(0\_)$, they are very difficult to be controlled in actual circuits, and cannot be an effective way to solve the HFO problems.

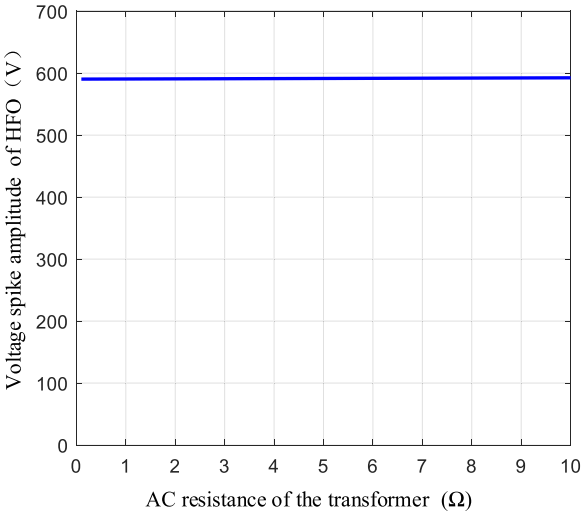

Fig. 12. Mathematical functional relationship between the VSA of HFO (A) and the ac resistance of the transformer (r) in the DAB prototype.

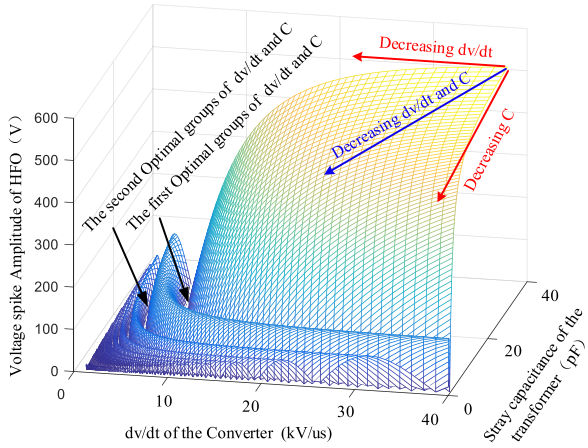

Fig. 13. Nonlinear relationship between the VSA of HFO, *dv/dt* of the converter and the stray capacitance of transformer.

F. Comprehensive Analysis of HFO

From the above analysis, it can be seen that the stray capacitance of the transformer (C) and the *dv/dt* of the converter (k) are the key influencing factors of the HFO. The HFO can be eliminated by optimizing these two factors in a specific DAB converter. However, the nonlinear relationship between the VSA of HFO and these influencing factors makes it very complicated to seek an effective method to mitigate the VSA of HFO in a specific DAB prototype. A 3-D figure, as shown in Fig. 13, can be drawn from (28) to show this nonlinear relationship.

It can be seen from Fig. 13 that the *dv/dt* of the DAB converter and the stray capacitance of the transformer is not the smaller the better to mitigate the VSA of HFO. As a matter of fact, there are several groups of optimal *dv/dt* and C to mitigate the VSA of HFO to a minimum value, which is different from the traditional ideas. On the other hand, when a higher *dv/dt* is generated in a DAB converter, a smaller stray capacitance of the transformer will be needed to mitigate the VSA of HFO; similarly, when a higher stray capacitance of the transformer is generated, a smaller *dv/dt* will be needed to mitigate the VSA of HFO. Therefore, the traditional methods of merely reducing the stray capacitance of the transformer or the *dv/dt* of the converter (as shown by the red line in Fig. 13), face great challenges especially when the WBG switching devices and nanocrystalline transformer cores are adopted in the DAB converters, because a higher *dv/dt* of the converter and a higher stray capacitance of the transformer will be generated with these advanced new materials. The best way to mitigate the VSA of HFO is to reduce the *dv/dt* of the converter and the stray capacitance of the transformer at the same time as shown by the blue line in Fig. 13.

IV. Proposed Elimination Method of HFO

To effectively mitigate the VSA of HFO, the mathematical relationship between the *dv/dt* of the converter and the stray capacitance of the transformer to mitigate the VSA of HFO to a minimum needs to be further deduced. The first-order derivative of the VSA (A_1) with respect to the voltage changing time of t_0 can be derived as follows, where the initial states of the circuit are ignored:

$$\frac{dA_1}{dt_0} = 1 + e^{-2\alpha t_0}(1+\alpha t_0) + e^{-\alpha t_0}\left[-2\cos(\beta t_0) + \alpha t_0\cos(\beta t_0) + \beta t_0 \sin(\beta t_0)\right]. \tag{29}$$

A simplified equation can be derived as follows when making the first-order derivative equal to zero and considering the inequality of $\alpha t_0 \ll 1$, $e^{-\alpha t_0} \approx 1$ for a DAB converter:

$$\frac{dA_1}{dt_0} = 2 - 2\cos(\beta t_0) + \beta t_0 \sin(\beta t_0) = 0. \tag{30}$$

A special solution of (30) can be deduced as follows:

$$t_0 = \frac{2n\pi}{\beta}, (n \in N^*). \tag{31}$$

When substituting the angular frequency of β with the oscillation period of t_{HFO} shown in (32), the special solution of (31) can be simply expressed as (33)

$$\beta = 2\pi f_{\mathrm{HFO}} = \frac{2\pi}{t_{\mathrm{HFO}}} \tag{32}$$

$$t_0 = n t_{\mathrm{HFO}}, (n \in N^*) \tag{33}$$

where t_0 is the voltage changing time of *dv/dt*, t_{HFO} is the oscillation cycle and f_{HFO} is the oscillation frequency.

The functional relationship between the VSA of HFO, the voltage changing time of *dv/dt* (t_0) and the oscillation cycle (t_{HFO}) can be seen more clearly by a 3-D figure as shown in Fig. 14, which is drawn based on (28), (33) and the circuit parameters in Section V. It can be seen that the VSA of HFO is almost reduced to 0 V when the voltage changing time of *dv/dt* (t_0) is an integer multiple times of the oscillation cycle (t_{HFO}), as shown by the red line in Fig. 14, which is consistent with the special solution of (33). It means that the HFO problems of the DAB converter can been perfectly solved under such circuit conditions. Therefore, an elimination method of HFO by equating the voltage changing time of *dv/dt* (t_0) to the oscillation

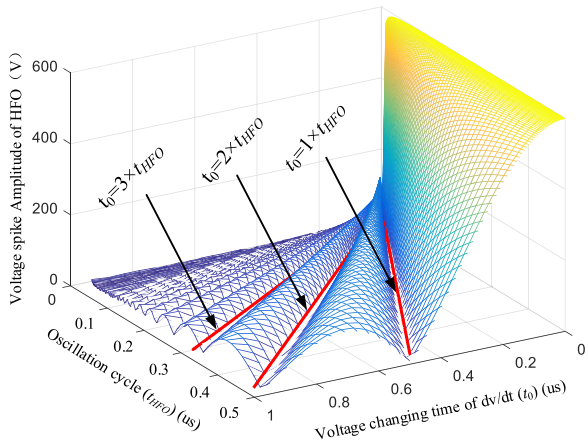

Fig. 14. Functional relationship between the VSA of HFO, the voltage changing time of *dv*/*dt* and the oscillation cycle.

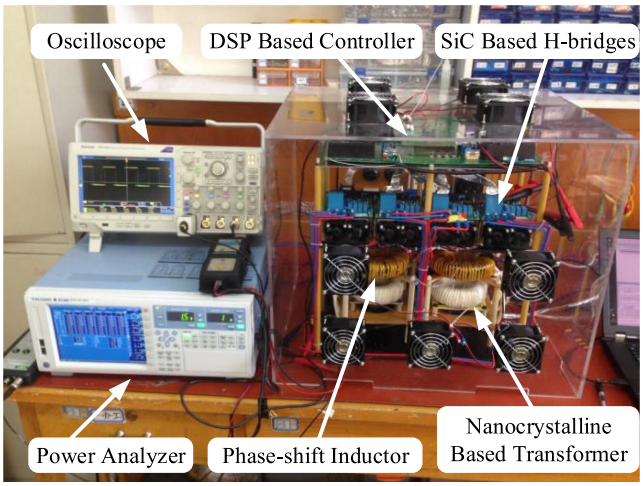

Fig. 15. A 6.6-kW DAB prototype build with WBG switching devices and nanocrystalline transformer cores.

cycle (t_{HFO}) can be reasonably proposed in this article, which guarantees the minimum VSA of HFO mathematically, and much easy to be implemented in a specific DAB converter.

V. Experimental Verification

A. Experimental Prototypes With WBG Devices and Nonocrystalline Transformer

In order to verify the proposed elimination method of HFO, a 6.6-kW DAB prototype with WBG switching devices and nanocrystalline transformer cores are built. The specifications and parameters of the DAB prototype are listed in Table I, and the photograph of the DAB prototype is shown in Fig. 15. In the DAB prototype, the high-speed SiC-MOSFETs of CREE-C2M0040120D are adopted as the switching devices, and the Fe-based nanocrystalline alloys of VAC VITROPERM 500F-W342 are adopted as the high-frequency transformer cores, which ensuring a higher efficiency under high switching frequency operating conditions of the DAB converter.

TABLE III
Experiment Specifications With Different Stray Capacitances of the Transformer

Transformer	#1	#2	#3
Layers	2	1	1
Insulation	Polyimide	Silica gel	Air
C	199.4 pF	102.4 pF	78.2 pF
f_{HFO}	2.0 MHz	2.86 MHz	3.2 MHz
t_{HFO}	500 ns	350 ns	312 ns
dv/dt	46 kV/us;	46 kV/us;	46 kV/us
t0	26 ns	26 ns	26 ns
VSA	690 V	460 V	440 V

B. Reducing the Stray Capacitance of the Transformer

A typical elimination method of HFO is to reduce the stray capacitance of the transformer. In this article, three different transformers with different winding layers and insulation materials are designed to reduce stray capacitances sequentially. The stray parameters are experimentally extracted by impedance characteristics method [25] listed in Table II, and the photographs of the transformers are shown in Fig. 16.

In transformer #1, there are two layers for the primary and secondary windings. Polyimide tapes with the relative permittivity equals to 3 are used as the insulation materials between layers. Due to the large number of transformer winding layers, the significantly increased electric field energy between layers of the transformer boosts the stray capacitance of the transformer obviously.

In transformer #2, the layers of the primary and secondary windings are reduced to 1, which greatly decreases the electric field energy between layers of the transformer, and a much lower stray capacitance can be achieved. In order to achieve a good heat dissipation performance, thermally conductive silica gel is used to fill the gaps between the turns of the transformer #2. However, the relative permittivity of the thermally conductive silica gel can reach up to 20, which can increase the electric field energy between turns and lead to a relatively large stray capacitance.

In transformer #3, the primary and secondary windings have a single layer, and the gaps between turns of the winding are filled with air. A minimum stray capacitance can be achieved by the single layer of the transformer winding and the minimum relative permittivity of the insulation material, because much of the electric field energy between layers and turns of the transformer is eliminated.

The voltage waveforms of U_p in the experiment are shown in Fig. 17 with three different transformers adopted. The VSA of HFO together with the other experiment specifications under different stray capacitances of the transformer are shown in Table III.

It can be seen that compared to transformer #1, the stray capacitance of the transformer #3 can be reduced to 39% (from 199.4 to 78.2 pF) by optimizing the physical structures of the transformer. The oscillation frequency of f_{HFO} increases from 2.0 to 3.2 MHz, and the VSA of HFO decreases from 720 to 440 V, that is, a 36.2% reduction of the VSA can be achieved by

(a) (b) (c)

Fig. 16. Three different transformers with different stray capacitances. (a) Transformer #1. (b) Transformer #2. (c) Transformer #3.

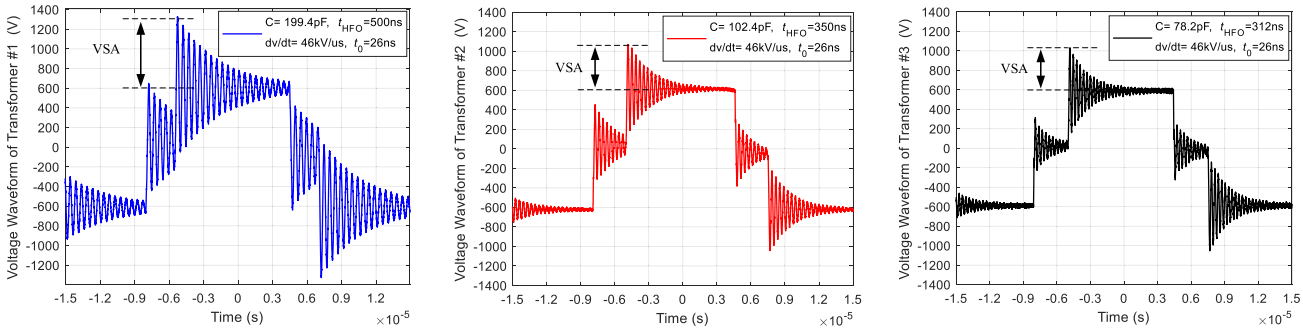

(a) (b) (c)

Fig. 17. Voltage waveforms of the transformer (U_p) in the experiment. (a) Transformer #1. (b) Transformer #2. (c) Transformer #3.

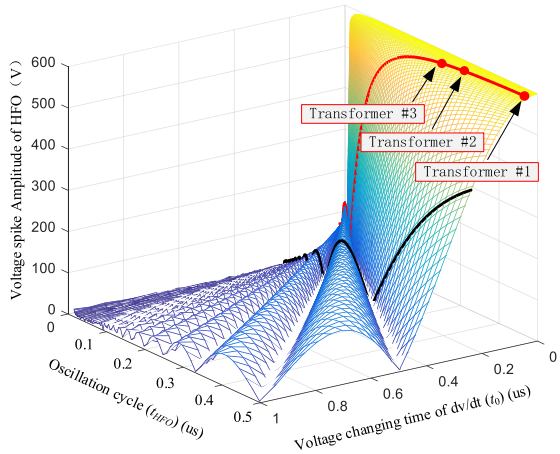

Fig. 18. HFO elemination by reducing stray capacitances of the transformer.

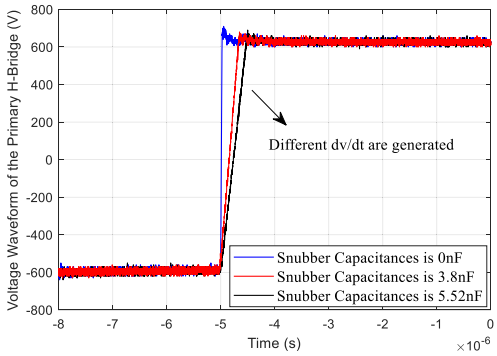

Fig. 19. Different *dv*/*dt* are generated in the experiment by connecting different snubber capacitances to the power devices.

optimizing the physical structures of the transformer. However, the HFO in the DAB prototype cannot be completely eliminated by reducing the stray capacitance of the transformer in the experiment.

It is clearly revealed by the red curve in Fig. 18 that the VSA of HFO cannot be mitigated effectively when an extremely high *dv*/*dt* (a small t_0) is generated, which means that the traditional method of reducing the stray capacitance of the transformer to eliminate the HFO is not suitable when fast switching devices utilized in the converter.

Only when the *dv*/*dt* is small enough, in conditions such as the low-speed switching devices (like Si-IGBT) are used in the converter, the method of reducing the stray capacitance of the transformer can be an effective way for HFO elimination, as the black curve demonstrated in Fig. 18.

C. Reducing the dv/dt of the Converter

It is well recognized that the *dv*/*dt* of the DAB converter in the experiment usually have a small difference due to the tolerance of the parasitic capacitance of power devices. However, when a relative larger snubber capacitance (compared with the parasitic capacitance) is parallel-connected with the power devices, this

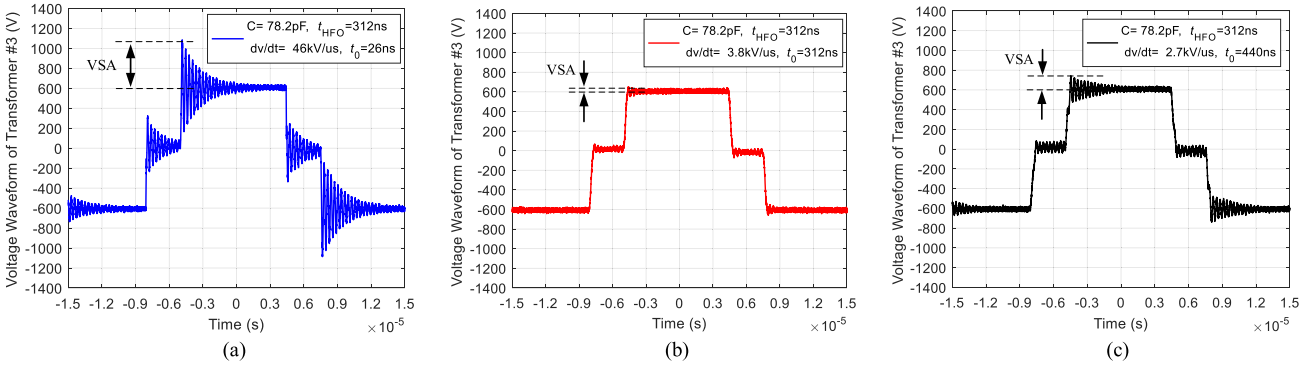

Fig. 20. Experimental voltage waveforms of the transformer by reducing the *dv/dt* of the converter: (a) *dv/dt* = 46 kV/us; (b) *dv/dt* = 3.8 kV/us; (c) *dv/dt* = 2.7 kV/us

TABLE IV
EXPERIMENTAL SPECIFICATIONS WITH DIFFERENT *DV/DT* OF THE CONVERTER

C_{parall}	0 nF	3.8 nF	5.52 nF
C	78.2 pF	78.2 pF	78.2 pF
f_{HFO}	3.2 MHz	3.2 MHz	3.2 MHz
t_{HFO}	312 ns	312 ns	312 ns
dv/dt	46 kV/us	3.8 kV/us	2.7 kV/us
t_0	26 ns	312 ns	440 ns
VSA	440 V	22 V	150 V

small difference can be ignored because the *dv/dt* of the DAB converter will be mainly determined by the snubber capacitance. Fig. 19 shows the *dv/dt* generated with different snubber capacitances connected with the power device in the experiment (the parasitic output capacitance of power devices is 0.15 nF obtained from the device datasheet).

It can be seen from Fig. 19 that the *dv/dt* of the DAB converter can be regulated by connecting different snubber capacitances to the power devices. Actually, the functional relationship between *dv/dt* and the paralleled snubber capacitance of C_{parall} can be derived in (34) when parallel-connected snubber capacitance is much larger than parasitic capacitance [31]

$$K = \frac{1}{C_{\mathrm{parall}}} |i(t)| \tag{34}$$

where $i(t)$ is the instant current of the H-bridge, which can be determined by (35) while taking the secondary H-bridge as an example

$$|i(t)| = \frac{U_{\mathrm{dc2}}/n + (2D-1)U_{\mathrm{dc1}}}{4f_s(L_{\mathrm{ph1}} + L_{\mathrm{ph2}})}. \tag{35}$$

In this article, different *dv/dt* are generated by regulating the snubber capacitance of the power devices under rated power. The experimental voltage waveforms of U_p, as shown in Fig. 20, with different *dv/dt* are generated. The VSA of HFO together with the other experiment specifications under different *dv/dt* are shown in Table IV.

It can be seen from Fig. 20 that the VSA of the HFO is up to 440 V when the *dv/dt* of the converter is 46 kV/μs, and will decrease to 22 V when the *dv/dt* is reduced to 3.8 kV/μs, while inversely goes up to about 150 V when the *dv/dt* is further reduced to 2.7 kV/μs. Therefore, the *dv/dt* of the converter is

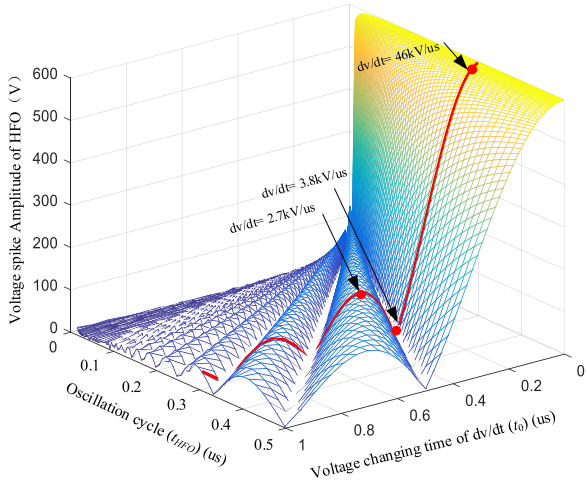

Fig. 21. HFO elimination by reducing the *dv/dt* (or increasing the t_0) of the DAB converter.

not the smaller the better to mitigate the HFO, which verifies the theoretical analysis in Section III.

In fact, as is depicted by the red curve in Fig. 21, the VSA of HFO can be mitigated effectively by reducing the *dv/dt* to 3.8 kV/μs, which ensures the optimal working conditions of the HFO elimination that the voltage changing time of *dv/dt*(t_0) equals to the oscillation cycle (t_{HFO}). However, the method of merely reducing the *dv/dt* of the converter to eliminate the HFO is not an feasible method when an extremely larger stray capacitance of the transformer is generated, because a much larger snubber capacitance is needed to be connected with the power devices to generate a much lower *dv/dt* (or a much larger t_0), leading to an extension of switching dead time for the converters. It is not permitted especially in higher switching frequency DAB converters, because the maximum switching frequency of the converter can be greatly reduced.

D. Proposed Elimination Method of HFO

The experimental verification of the proposed elimination method of HFO is carried out with three different transformers adopted respectively in a 6.6-kW DAB prototype. First, the oscillation cycle of t_{HFO} is calculated by (14) and (32) based on the stray parameters shown in Table II and the parameters of

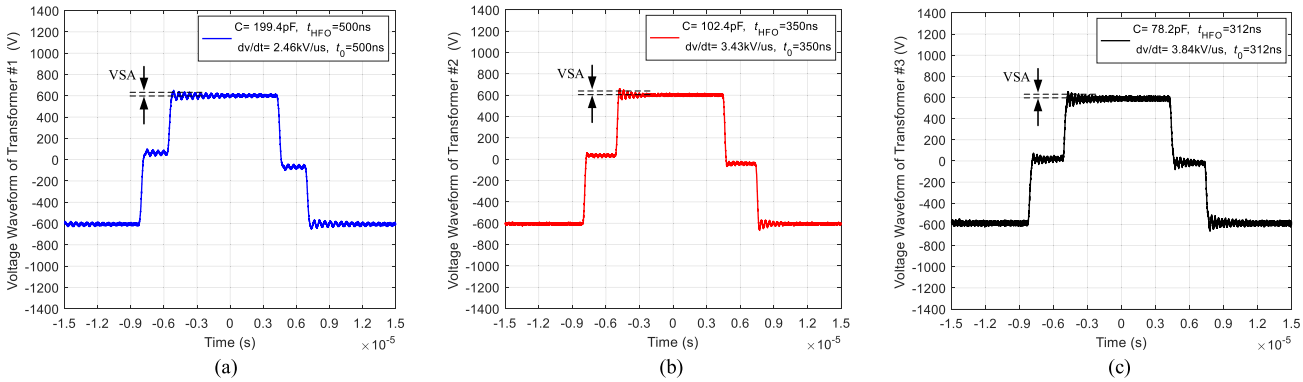

Fig. 22. Experimental voltage waveforms of the transformer with the proposed elimination method of HFO. (a) Transformer #1. (b) Transformer #2. (c) Transformer #3.

TABLE V
EXPERIMENTAL SPECIFICATIONS WITH THE PROPOSED ELIMINATION METHOD OF HFO

Transformer	#1	#2	#3
C_{parall}	6.0 nF	4.3 nF	3.8 nF
C	199.4 pF	102.4 pF	78.2 pF
f_{HFO}	2.0 MHz	2.86 MHz	3.2 MHz
t_{HFO}	500 ns	350 ns	312 ns
dv/dt	2.4 kV/us	3.4 kV/us	3.8 kV/us
t_0	500 nS	350 nS	312 nS
VSA	20 V	20 V	22 V

DAB converter shown in Table I. Then the snubber capacitances of C_{parall} are calculated from (7), (34), (35) by equating the voltage changing time of dv/dt (t_0) equals to the oscillation cycle (t_{HFO}). The calculated parameters together with the VSA of HFO in the experiment are listed in Table V. The experimental voltage waveforms of the transformer (U_p) are shown in Fig. 22.

Compared with the voltage waveforms of the transformer shown in Fig. 17 and the VSA of HFO in Table III, the VSA of HFO can be reduced by more than 95% shown in Fig. 22 and Table V. It can be seen more clearly by the red line shown in Fig. 23 that the minimum VSA of HFO can be achieved by equating the voltage changing time of dv/dt (t_0) to the oscillation cycle (t_{HFO}), which means that the HFO problems can be effectively solved in the experiment when the proposed elimination method of HFO is adopted in this article.

E. Efficiency of the DAB Converter

In this article, in order to eliminate the HFO of the DAB converter, the dv/dt of the converter and the stray capacitance of the transformer are regulated simultaneously to ensure that the voltage changing time of dv/dt equates to the oscillation cycle. However, the slowing dv/dt by increasing the gate resistances or snubber capacitances of the switching devices usually results in a change in switching loss or converter efficiency. Further experiments are carried out under rated power with different gate resistances and snubber capacitances. The measured dv/dt and efficiency of the DAB converter are shown in Fig. 24.

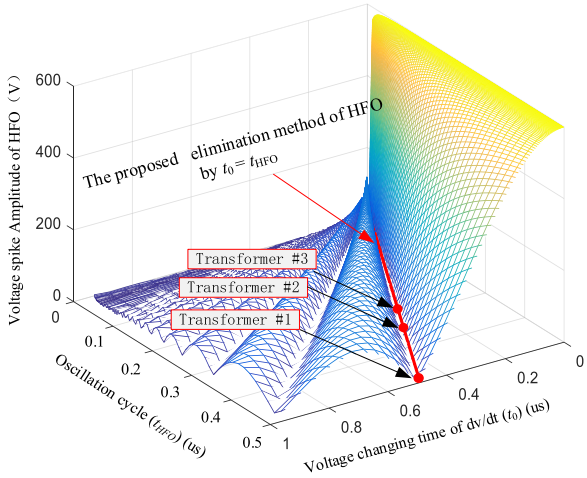

Fig. 23. Proposed elimination method of HFO by equating the voltage changing time of dv/dt (t_0) and the oscillation cycle (t_{HFO}).

It can be seen from Fig. 24(a) that the dv/dt of the converter can be reduced by increasing the gate resistances or snubber capacitances to the power devices. However, when the snubber capacitances are larger than 1 nF, dv/dt is mainly determined by the snubber capacitance, and has little relationship on the gate resistances.

Fig. 24(b) shows that the efficiency of the converter increases as the snubber capacitance increases, but decreases as the gate resistance increases. When the snubber capacitance is large enough, the efficiency is mainly determined by the snubber capacitance and has less relationship with the gate resistances. The overall efficiency of the DAB converter goes up to over 98.2% with the snubber capacitances larger than 3 nF.

Actually, the efficiency improvement of the DAB converter with the snubber capacitances is mainly due to the soft-switching status of the switching devices. When a snubber capacitance is connected in parallel with the power device, the voltage of the power device will be clamped by the snubber capacitor. Since the capacitor voltage cannot be changed suddenly, the voltage of the switching device remains almost zero when the switching device is turned OFF, which means that the turn-OFF switching loss of the power devices is significantly reduced, and a quasi-zero voltage condition is achieved when the power

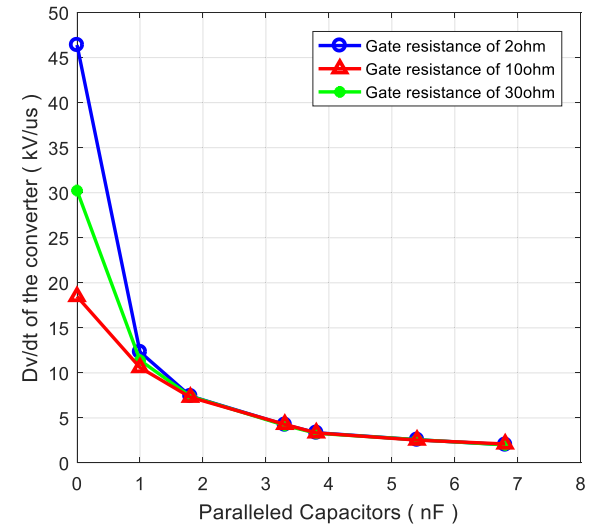

Fig. 24. *DV/DT* and efficiency of the DAB converter with different MOSFET gate resistances and snubber capacitances under rated power. (a) Dv/dt of the DAB converter. (b) Efficiency of the DAB converter.

device is turned OFF [32]. On the other hand, since the DAB converter has a ZVS-ON instinct, i.e., the energy in the snubber capacitance can be recycled before the device is turned ON, the overall efficiency of the DAB converter increases as the snubber capacitance increases. However, when a DAB converter loses ZVS-ON characteristic under certain load and gain conditions, the energy on the snubber capacitance will be dissipated on the switching devices and the overall efficiency of the DAB converter will decrease as the snubber capacitance increases. The soft-switching characteristics of a DAB converter with snubber capacitances connected in parallel with the power devices are further discussed in [32].

VI. Conclusion

In this article, a comprehensive analysis, design, and optimal methodology of HFO for DAB with WBG switching devices and nanocrystalline transformer cores is proposed. Based on the theoretical analysis, this article points out for the first time that the traditional method of decreasing the stray capacitance of the transformer to eliminate the HFO is not suitable for high *dv/dt* occasions when fast switching devices are utilized in the converter. Correspondingly, a novel elimination method of HFO by equating the voltage changing time of *dv/dt* and the oscillation cycle is proposed theoretically, through which the minimum VSA of HFO can be achieved mathematically. Experimental verification of the proposed method are carried out on a 6.6-kW DAB prototype with three different transformers employed, respectively, which shows that the VSA of the HFO can be reduced by 95% when the proposed elimination method are adopted, whereas a merely 36.2% reduction of the VSA can be achieved with the traditional method of decreasing the stray capacitance of the transformer, which means that the HFO in DAB converters can be effectively eliminated with the proposed elimination method adopted in this article.

References

[1] B. Zhao, Q. Song, W. Liu, and Y. Sun, "Overview of dual-active-bridge isolated bidirectional DC–DC converter for high-frequency-link power-conversion system," *IEEE Trans. Power Electron.*, vol. 29, no. 8, pp. 4091–4106, Aug. 2014.

[2] B. Zhao, Q. Song, and W. Liu, "Power characterization of isolated bidirectional dual-active-bridge DC–DC converter with dual-phase-shift control," *IEEE Trans. Power Electron.*, vol. 27, no. 9, pp. 4172–4176, Sep. 2012.

[3] W. Shen, F. Wang, D. Boroyevich, and C. W. Tipton IV, "High-density nanocrystalline core transformer for high-power high-frequency resonant converter," *IEEE Trans. Ind. Appl.*, vol. 44, no. 1, pp. 213–222, Jan./Feb. 2008.

[4] W. Shen, F. Wang, D. Boroyevich, and C. W. Tipton, "High power density nanocrystalline core transformer design for resonant converter systems," in *Proc. 40th IAS Annu. Meeting. Rec. Ind. Appl. Conf.*, 2005, pp. 2216–2222.

[5] B. Zhao, Q. Song, W. Liu, and Y. Sun, "Dead-time effect of the high-frequency isolated bidirectional full-bridge DC–DC converter: Comprehensive theoretical analysis and experimental verification," *IEEE Trans. Power Electron.*, vol. 29, no. 4, pp. 1667–1680, Apr. 2014.

[6] L. Dalessandro, F. da Silveira Cavalcante, and J. W. Kolar, "Self-capacitance of high-voltage transformers," *IEEE Trans. Power Electron.*, vol. 22, no. 5, pp. 2081–2092, Sep. 2007.

[7] C. Liu, L. Qi, X. Cui, Z. Shen, and X. Wei, "Wideband mechanism model and parameter extracting for high-power high-voltage high-frequency transformers," *IEEE Trans. Power Electron.*, vol. 31, no. 5, pp. 3444–3455, May 2016.

[8] R. Chattopadhyay, M. A. Juds, G. Gohil, S. Gulur, P. R. Ohodnicki, and S. Bhattacharya, "Optimized design for three port transformer considering leakage inductance and parasitic capacitance," in *Proc. IEEE Energy Convers. Congr. Expo.*, 2017, pp. 3247–3254.

[9] Z. Qin, Z. Shen, and F. Blaabjerg, "Modelling and analysis of the transformer current resonance in dual active bridge converters," in *Proc. IEEE Energy Convers. Congr. Expo.*, 2017, pp. 4520–4524.

[10] R. Chattopadhyay, M. A. Juds, P. R. Ohodnicki, and S. Bhattacharya, "Modelling, design and analysis of three limb high frequency transformer including transformer parasitics, for SiC mosfet based three port DAB," in *Proc. 42nd Annu. Conf. IEEE Ind. Electron. Soc.*, 2016, pp. 4181–4186.

[11] B. Farhangi and H. A. Toliyat, "Modeling isolation transformer capacitive components in a dual active bridge power conditioner," in *Proc. IEEE Energy Convers. Congr. Expo.*, 2013, pp. 5476–5480.

[12] M. A. Saket, N. Shafiei, and M. Ordonez, "LLC converters with planar transformers: Issues and mitigation," *IEEE Trans. Power Electron.*, vol. 32, no. 6, pp. 4524–4542, Jun. 2017.

[13] N. Wang, H. Jia, M. Tian, Z. Li, G. Xu, and X. Yang, "Impact of transformer stray capacitance on the conduction loss in a GaN-based LLC resonant converter," in *Proc. IEEE 3rd Int. Future Energy Electron. Conf.*, 2017, pp. 1334–1338.

[14] Z. Ouyang, O. C. Thomsen, and M. A. E. Andersen, "Optimal design and tradeoff analysis of planar transformer in high-power DC–DC converters," *IEEE Trans. Ind. Electron.*, vol. 59, no. 7, pp. 2800–2810, Jul. 2012.

[15] J. Biela and J. W. Kolar, "Using transformer parasitics for resonant converters—A review of the calculation of the stray capacitance of transformers," *IEEE Trans. Ind. Appl.*, vol. 44, no. 1, pp. 223–233, Jan./Feb. 2008.
[16] Z. De Grève, O. Deblecker, and J. Lobry, "Numerical modeling of capacitive effects in HF multiwinding transformers—Part I: A rigorous formalism based on the electrostatic equations," *IEEE Trans. Magn.*, vol. 49, no. 5, pp. 2017–2020, May 2013.
[17] C. Liu, L. Qi, X. Cui, and X. Wei, "A terminal capacitance method for analyzing global capacitive effects of magnetic components," *IEEE Trans. Electromagn. Compat.*, vol. 59, no. 4, pp. 1161–1170, Aug. 2017.
[18] G. Liang, H. Sun, X. Zhang, and X. Cui, "Modeling of transformer windings under very fast transient overvoltages," *IEEE Trans. Electromagn. Compat.*, vol. 48, no. 4, pp. 621–627, Nov. 2006.
[19] M. M. Kane and S. V. Kulkarni, "MTL-based analysis to distinguish high-frequency behavior of interleaved windings in power transformers," *IEEE Trans. Power Del.*, vol. 28, no. 4, pp. 2291–2299, Oct. 2013.
[20] H. Y. Lu, J. Guo Zhu, and S. Y. R. Hui, "Experimental determination of stray capacitances in high frequency transformers," *IEEE Trans. Power Electron.*, vol. 18, no. 5, pp. 1105–1112, Sep. 2003.
[21] B. Cogitore, J. P. Keradec, and J. Barbaroux, "The two-winding transformer: An experimental method to obtain a wide frequency range equivalent circuit," *IEEE Trans. Instrum. Meas.*, vol. 43, no. 2, pp. 364–371, Apr. 1994.
[22] IEEE Recommended Practice for Testing Electronic Transformers and Inductors, IEEE Standard 389-1990, 28 Aug. 1990, pp. 1–64.
[23] J. Biernacki and D. Czarkowski, "High frequency transformer modeling," in *Proc. IEEE Int. Symp. Circuits Syst.*, 2001, pp. 676–679.
[24] R. Prieto, R. Asensi, J. A. Cobos, O. Garcia, and J. Uceda, "Model of the capacitive effects in magnetic components," in *Proc. Power Electron. Specialist Conf.*, 1995, pp. 678–683.
[25] C. Liu, L. Qi, X. Cui, and X. Wei, "Experimental extraction of parasitic capacitances for high-frequency transformers," *IEEE Trans. Power Electron.*, vol. 32, no. 6, pp. 4157–4167, Jun. 2017.
[26] Z. Qin, Z. Shen, and F. Blaabjerg, "Modelling and analysis of the transformer current resonance in dual active bridge converters," in *Proc. IEEE Energy Convers. Congr. Expo.*, 2017, pp. 4520–4524.
[27] Z. Qin, Z. Shen, F. Blaabjerg, and P. Bauer, "Modelling, analysis and mitigation of the transformer current ringing in dual active bridge converters," in *Proc. IEEE Energy Convers. Congr. Expo.*, 2018, pp. 650–655.
[28] M. Borage, K. V. Nagesh, M. S. Bhatia, and S. Tiwari, "Design of LCL-T resonant converter including the effect of transformer winding capacitance," *IEEE Trans. Ind. Electron.*, vol. 56, no. 5, pp. 1420–1427, May 2009.
[29] T. C. W. McLyman, "Winding capacitance and leakage inductance," in *Transformer Inductor Design Handbook*, 3rd ed. New York, NY, USA: CRC Press, 2004, pp. 427–440.
[30] P. Thummala, H. Schneider, Z. Zhang, and M. A. E. Andersen, "Investigation of transformer winding architectures for high-voltage (2.5 kV) capacitor charging and discharging applications," *IEEE Trans. Power Electron.*, vol. 31, no. 8, pp. 5786–5796, Aug. 2016.
[31] B. Cui, P. Xue, and X. Jiang, "Elimination of high frequency oscillation in dual active bridge converters by dv/dt optimization," *IEEE Access*, vol. 7, pp. 55554–55564, 2019.
[32] C. Fontana, M. Forato, K. Kumar, M. T. Outeiro, M. Bertoluzzo, and G. Buja, "Soft-switching capabilities of SAB vs. DAB converters," in *Proc. 41st Annu. Conf. IEEE Ind. Electron. Soc.*, 2015, pp. 003485–003490.

Bin Cui (Member, IEEE) was born in Jinan, China. He received the B.S. degree in electrical engineering from Harbin Institute of Technology, Harbin, China, in 2009, the M.S. degree in electrical engineering from Fuzhou University, Fuzhou, China, in 2012, and the Ph.D. degree form the Department of Electrical Engineering, Tsinghua University, Beijing, China, in 2019.

He is currently a Postdoctoral Fellow in electrical engineering with Tsinghua University. His research interests include high-frequency dc–dc converters, high-frequency transformers, high power converters, and flexible dc transmission and distribution systems.

Hongliang Shi (Student Member, IEEE) was born in Hubei, China, in 1983. He received the B.S. degree from JiangNan University, Wuxi, China, in 2004, the master's degree from Huazhong University of Science and Technology, Wuhan, China, in 2007, and the Ph.D. degree from Tsinghua University, Beijing, China, in 2016, both in electrical engineering.He is currently a Senior Engineer with the CRRC Zhuzhou Electric Co. Ltd. His research interests include high-frequency and high power converter design, the modeling and applications of SiC MOSFET devices, and optimal design of medium frequency transformers and inductors.

Qianhao Sun (Student Member, IEEE) was born in Shanxi, China, in 1993. He received the B.S. degree from Northeast Electric Power University, Jilin, China, in 2014, and the M.S. and Ph.D. degrees from Tsinghua University, Beijing, China, in 2017 and 2020, respectively, all in electrical engineering.

From May to November, 2019, he was a Visiting Ph.D. Student with Cardiff University, Cardiff, U.K. His research interests include the high-frequency dc–dc converters and the flexible dc transmission and distribution systems.

Xueteng Tang was born in Shandong, China, in 1986. He received the B.S. degree from the Department of Electrical Engineering, Beihua University, Jilin, China, in 2008.

He is currently an Engineer with the Energy Internet Research Institute, Tsinghua University, Beijing, China. His research interests include high power converters and flexible dc transmission and distribution systems.

Lucheng Hong (Member, IEEE) was born in Nantong, China, in 1985. He received a B.S. degree from the School of Electrical Engineering, Southeast University, Nanjing, China, in 2007 and the Ph.D. degree from the Department of Electrical Engineering, Tsinghua University, Beijing, China, in 2013, both in electrical engineering.

He is currently an Associate Professor with the School of Electrical Engineering, Southeast University, Nanjing, China. His research interests include analysis on power load and consumption characteristics, distributed power system stability, and power quality.

Biao Zhao (Senior Member, IEEE) was born in Hubei, China, in 1987. He received the B.S. degree from the Department of Electrical Engineering, Dalian University of Technology, Dalian, China, in 2009, and the Ph.D. degree form the Department of Electrical Engineering, Tsinghua University, Beijing, China, in 2014.

He is currently an Associate Professor with the Department of Electrical Engineering, Tsinghua University, Beijing, China. His research interests include high power converters, high power semiconductor devices, and flexible dc transmission and distribution systems.

Dr. Zhao is a Senior Member of the Chinese Society for Electrical Engineering and the Chinese Electro-Technical Society.